

Article

Study of La Doping on the Electronic Structure and Magneto-Optical Properties of ZnO by GGA+U Method

Qiao Wu ¹, Bohang Zhang ², Gaihui Liu ², Jing Ning ², Tingting Shao ², Fuchun Zhang ^{2,*} and Suqin Xue ^{1,*}¹ Network Information Center, Yan'an University, Yan'an 716000, China² School of Physics and Electronic Information, Yan'an University, Yan'an 716000, China

* Correspondence: yadxzfc@yau.edu.cn (F.Z.); ydxsq@yau.edu.cn (S.X.)

Abstract: Based on the density functional theory, the effect of rare-earth La doping at different concentrations on the electronic structure, optical properties, and magnetic properties of ZnO was calculated by using the GGA+U method under the condition of spin polarization. The calculation results show that the cell of a La-doped ZnO system is distorted, resulting in a formation energy less than zero, in which case it is easy to dope. After La doping, the band gap narrows, the Fermi level enters the conduction band, and the excess carriers induced by La atoms degenerate to form n-type degenerate semiconductor materials. In the visible light region, a blue shift in the optical absorption edge of the La-doped ZnO system causes an increased average static dielectric constant, stronger polarization ability, stronger binding ability on charges, and the photoconductivity of the doped ZnO system is improved. The magnetic moment of the La-doped ZnO system is zero, so it is not magnetic.

Keywords: rare-earth element; La; ZnO doping; first-principle; optical properties; magnetic properties



Citation: Wu, Q.; Zhang, B.; Liu, G.; Ning, J.; Shao, T.; Zhang, F.; Xue, S. Study of La Doping on the Electronic Structure and Magneto-Optical Properties of ZnO by GGA+U Method. *Crystals* **2023**, *13*, 754. <https://doi.org/10.3390/cryst13050754>

Academic Editor: Alessandra Toncelli

Received: 17 March 2023

Revised: 23 April 2023

Accepted: 26 April 2023

Published: 2 May 2023



Copyright: © 2023 by the authors. Licensee MDPI, Basel, Switzerland. This article is an open access article distributed under the terms and conditions of the Creative Commons Attribution (CC BY) license (<https://creativecommons.org/licenses/by/4.0/>).

1. Introduction

At room temperature, ZnO has a direct wide band gap (3.37 eV), a large exciton binding energy (60 meV), excellent electronic and piezoelectric properties, and is widely used in the fields of optoelectronics, spintronics, and other materials [1–3]. At present, impurity doping is an effective method to change the electronic, optic, magnetic, and other properties of semiconductor materials. Domestic and foreign research groups have carried out a large number of experimental studies and theoretical calculations on 3d transition metal ions, rare-earth ions, non-magnetic ions, and other doped ZnO crystals [4,5]. Rare-earth ions have partially filled 4f shells and, if incorporated into ZnO matrixes, their intra-4f optical transitions become possible because of splitting induced by the crystal field of ZnO. Rare-earth-element-doped ZnO has a significant influence on its photoelectric and magnetic properties [6,7]. In terms of experimental research, Li et al. [7] have proposed that by coating silica shell on ZnO: Yb³⁺, Tm³⁺ nanocrystals, substantial photon avalanche is generated, which leads to efficient upconversion luminescence. Moreover, these ZnO nanoparticles have been successfully explored for fluorescence imaging of myocardial tissue. Yao et al. [8] studied rare-earth-ion-doped phosphors for dye-sensitized solar cell applications, and showed that RE-doped upconverters or downconverters serve as an excellent luminescent conversion material arising from their intra-4f transitions, which have been widely applied in photovoltaic devices. ZnO is one of the most commonly used host materials. Vettumperumal et al. [9] Er-doped a ZnO semiconductor structure that was prepared by the sol-gel method. It was found that a low-concentration of rare-earth-doped ZnO would not destroy the hexagonal structure of ZnO, and showed stronger exciton bonds than the intrinsic ZnO, and a greater transmission coefficient. In terms of theoretical calculations, Khuili et al. [10] studied the electronic, optic, and magnetic properties of ZnO doped with rare-earth elements (Tm, Yb, and Ce) using the density functional theory. The results showed that ZnO doped with rare-earth elements had a significant impact on the

photoelectric and magnetic properties of ZnO, which was mainly due to the existence of 4f electrons, and the conductivity was significantly improved after doping. Zhang et al. [11] studied the electronic structure and magnetic properties of rare-earth elements (La, Ce, Pr, Nd, and Eu) -doped ZnO by using the first-principle calculation method. The results showed that La-doped ZnO can produce a diamagnetic ground state, with the doping of La and Ce more stable than that of Pr, Nd, and Eu. The ground state of Pr-, Nd-, and Eu-doped ZnO has weak antiferromagnetism, while the ground state of Ce-doped ZnO has ferromagnetism. The above research and a few important applications indicate that it is scientific and significant to calculate the effect of rare-earth (La) doping with different concentrations on the electronic structure, optical properties, and magnetic properties of ZnO based on density functional theory in this paper, which can provide important theoretical guidance for the research and preparation of electronic devices with excellent magneto-optical properties.

In this work, we study orbital charge using the Mulliken population analysis method [12], which is calculated according to the formalism [13]. It is an important method to understand the bonding behavior of crystals. The analysis of the orbital charge number is used to describe the charge transfer after bonding, where positive and negative values indicate the loss and gain of the atom, respectively. However, the Hirshfeld partitioned charges are defined relative to the deformation density. The deformation density is the difference between the molecular and the unrelaxed atomic charge densities [14]. Natural bond orbital (NBO) analysis is a method to study hybridization and covalent effects in polyatomic molecular systems [15–17]. Compared with the Mulliken population analysis method, NBO methods give information about interactions in both filled and virtual orbital spaces that could enhance the analysis of intra- and intermolecular interactions, and all orbital details are mathematically chosen to include the highest possible percentage of the electron density. At the same time, it can avoid negative orbital occupancy, so the calculated results are more consistent with the experimental values. However, the Mulliken population analysis method has also been cited by many papers, and its calculation results can scientifically explain the test results.

2. Calculation Model and Method

2.1. Calculation Model

ZnO belongs to the hexagonal wurtzite structure, whose space group is P63m (No. 186), lattice constant $a = b = 0.325$ nm, $c = 0.520$ nm, $\alpha = \beta = 90^\circ$, and $\gamma = 120^\circ$ [18]. In this paper, the supercell model of intrinsic $\text{Zn}_{16}\text{O}_{16}$ ($2 \times 2 \times 2$) includes 16 O atoms and 16 Zn atoms; the supercell model of $\text{Zn}_{15}\text{La}_1\text{O}_{16}$ ($2 \times 2 \times 2$) includes 16 O atoms, 15 Zn atoms, and 1 La atom; and the supercell model of $\text{Zn}_{14}\text{La}_2\text{O}_{16}$ ($2 \times 2 \times 2$) include 16 O atoms, 14 Zn atoms, and 2 La atoms, as shown in Figure 1. We designed four different configurations for $\text{Zn}_{14}\text{La}_2\text{O}_{16}$ and the La sites in $\text{Zn}_{14}\text{La}_2\text{O}_{16}$ are shown in Figure 1c–f. The electronic structure, optical properties, and magnetic properties were calculated and analyzed on the basis of geometric structure optimization.

2.2. Calculation Method

In this study, the plane-wave pseudopotential approach and GGA+U [19] method were used, as implemented in the CASTEP [20] module of Material Studio 2020 software, which is based on the density functional theory (DFT), wherein, U is the coulomb potential. The exchange-correlation energy was described by the GGA-PBE [21]. Since the geometrical configurations of the La element play a significant role in determining the magnetic behavior of $\text{Zn}_{15}\text{La}_1\text{O}_{16}$ and $\text{Zn}_{14}\text{La}_2\text{O}_{16}$ [22]. So, it is crucial to obtain realistic geometries for the doped structures. We computed the value of Hubbard U via the linear response approach and confirm its validity [23]. When $U_{d-\text{Zn}} = 10.0$ eV, $U_{p-\text{O}} = 7.0$ eV, and $U_{f-\text{La}} = 6.0$ eV [24,25], the calculated band gap for ZnO was 3.34 eV, and the lattice parameters were $a = 3.269$ Å and $c = 5.272$ Å, which are in good agreement with the experimental values [26], overestimated by only 0.6% and 1.3%, respectively. This minor expansion in

lattice constants is attributed to the nature of the GGA in softening chemical bonds [27,28]. To obtain both speed and accuracy, the energy cut-off and k-point mesh were set to 800 eV and $4 \times 4 \times 2$, respectively. However, in this work, convergence testing was performed, by increasing the k-point mesh to $4 \times 4 \times 3$ and the energy cut-off to 930 eV. It was found that the total energy differs very little. Thus, the results were well-converged. The outer valence electron configurations selected for calculation were Zn-3d¹⁰4s², O-2s²2p⁴, and La-5d¹6s². Other orbital electrons were used as rump electrons for calculation. Spin polarization was used to treat electrons when calculating energy. Due to convergence issues, we set the computational parameters as the following: the energy tolerance is 5×10^{-6} eV/atom and the convergence criteria are 0.01 eV/Å, 0.02 GPa and 5×10^{-4} Å for maximum force, stress, and displacement, respectively.

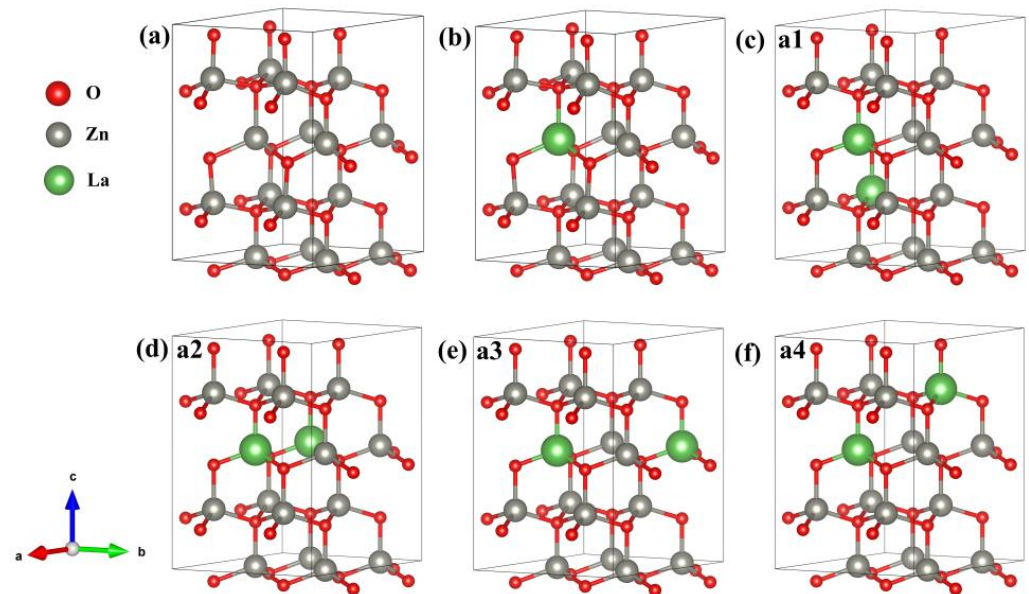


Figure 1. Calculation model. (a) $\text{Zn}_{16}\text{O}_{16}$, (b) $\text{Zn}_{15}\text{La}_1\text{O}_{16}$, (c) $\text{Zn}_{14}\text{La}_2\text{O}_{16}^{\text{a1}}$, (d) $\text{Zn}_{14}\text{La}_2\text{O}_{16}^{\text{a2}}$, (e) $\text{Zn}_{14}\text{La}_2\text{O}_{16}^{\text{a3}}$, (f) $\text{Zn}_{14}\text{La}_2\text{O}_{16}^{\text{a4}}$. Annotation: a1–a4 represents four different configurations for $\text{Zn}_{14}\text{La}_2\text{O}_{16}$.

3. Results and Discussion

3.1. Doping System Structure and Stability Analysis

The geometric structure of $\text{Zn}_{16}\text{O}_{16}$, $\text{Zn}_{15}\text{La}_1\text{O}_{16}$, and $\text{Zn}_{14}\text{La}_2\text{O}_{16}$ supercell models was optimized; the $\text{Zn}_{14}\text{La}_2\text{O}_{16}$ supercell model includes four different configurations. The cell parameters are listed in Table 1. It can be seen from the analysis that with the increase in La doping concentration, the lattice parameters, which include lengths and angles of the doped system distortion, indicate the lattice mismatch between the La^{3+} and ZnO lattice. By comparing the lattice parameters of the four different configurations of the $\text{Zn}_{14}\text{La}_2\text{O}_{16}$ supercell model, it is found that there is little difference between them. According to the theoretical analysis of quantum chemistry, the radius of La^{3+} ions (0.1032 nm) is greater than that of Zn^{2+} ions (0.074 nm), and the volume of the system will become larger after La^{3+} replaces Zn^{2+} . In addition, the repulsion between the surplus positive charges of La^{3+} is enhanced after doping, which leads to the larger volume of the system after doping impurities based on the above two reasons [29]. The experimental results of the reports [30,31] showed that the wurtzite ZnO is the only XRD detectable phase of the films. This might indicate that the La^{3+} cation entered into the ZnO lattice, and the lattice also expands with the increase in La content. It showed that the theoretical calculation results in this paper are in agreement with the experimental results.

Table 1. Cell parameters and formation energy after structural optimization of intrinsic ZnO and La-doped ZnO systems.

Model	a/Å	b/Å	c/Å	α	β	γ	V/Å ³	E_f /eV
Zn ₁₆ O ₁₆	6.821	6.821	10.942	90.00°	90.00°	120.00°	440.898	-
Zn ₁₅ La ₁ O ₁₆	6.909	6.909	10.979	90.00°	90.00°	119.99°	453.885	-6.505
Zn ₁₄ La ₂ O ₁₆ ^{a1}	7.056	7.064	10.758	90.00°	89.89°	120.01°	464.264	-12.519
Zn ₁₄ La ₂ O ₁₆ ^{a2}	7.232	7.090	10.459	90.06°	90.02°	120.64°	461.378	-11.962
Zn ₁₄ La ₂ O ₁₆ ^{a3}	7.091	7.091	10.457	89.93°	90.07°	118.65°	461.387	-11.956
Zn ₁₄ La ₂ O ₁₆ ^{a4}	7.096	7.096	10.568	89.99°	89.99°	119.97°	460.942	-12.496

Annotation: a1–a4 represents four different configurations for Zn₁₄La₂O₁₆.

In order to further test the stability of the doped system and the difficulty of La doping, the formation energy E_f of the doped system is calculated, which is listed in Table 1, and its expression is [32,33]

$$E_f = E_{(\text{ZnO} + \text{La})} - E_{\text{ZnO}} - n_{\text{La}}\mu_{\text{La}} + n_{\text{Zn}}\mu_{\text{Zn}} \quad (1)$$

wherein $E_{(\text{ZnO} + \text{La})}$ is the total energy of the doped system, E_{ZnO} is the total energy of the intrinsic ZnO with the same atomic number, n_{La} is the number of doped atoms La, n_{Zn} is the number of replaced Zn atoms, μ_{La} and μ_{Zn} are the chemical potential of the doped atoms La and Zn, respectively (when $T = 0$ K), and the total energy of an atom placed in the bulk structure La (P6₃/mmc) and Zn (P6₃/mmc) can be used to replace the chemical potential of doped La and Zn atoms. It can be seen from Table 1 that the formation energy E_f of the La-doped ZnO system is negative, indicating that doping is easier. Moreover, we calculated the formation energy of the four different configuration systems of Zn₁₄La₂O₁₆, respectively, the results show that the formation energy of the a1 configuration (Figure 1c) is the lowest, indicating that the a1 configuration is easier to form and the system is more stable. The electronic structure, optical properties, and magnetic properties that were calculated and analyzed of Zn₁₄La₂O₁₆ are mainly based on the a1 configuration.

3.2. Analysis of Energy Band Structure

The band gap width is the energy difference between the highest energy level of the occupied electron and the lowest energy level of the unoccupied electron. It is a key characteristic parameter that affects the optical property of semiconductor materials. Figure 2 shows the spin-up and spin-down energy band structure of the intrinsic ZnO and La-doped ZnO systems under the condition of spin polarization. The dotted line E_f is 0 eV Fermi surface. Figure 2a shows the energy band structure of Zn₁₆O₁₆. Analysis suggests that the band gap value of the intrinsic ZnO corrected by the GGA+U method is 3.34 eV, which is basically consistent with the experimental value of 3.37 eV [26], so the U parameter selected for calculation is reliable. In addition, both the top of the valence band and the bottom of the conduction band are located at the G point and the transition type is G-G, which indicate that the intrinsic ZnO is a direct band gap semiconductor.

Figure 2b,c show the energy band structure of Zn₁₅La₁O₁₆ and Zn₁₄La₂O₁₆. Analysis shows that the band gap value of Zn₁₅La₁O₁₆ is 3.16 eV, and the band gap value of Zn₁₄La₂O₁₆ is 2.90 eV. With the increase in the La atom doping concentration, the band gap decreases; this is consistent with the results obtained by R. Bomila et al. [34] using UV-VIS spectral data to determine that the band gap energy decreases with the increase in the La doping concentration. The decrease in the band gap is beneficial to improve the optical and electron transport characteristics of the doping system, which is explained by the combined action of the Burstein–Moss effect and the renormalization effect. After the doping of La atoms, the energy band voltage decreases, indicating that the effective mass of electrons in the energy band increases, the degree of localization increases, the atomic orbital expansion weakens, and the number of the conduction band and valence band energy bands increases significantly. The energy band structure is more compact.

The doping of La atoms enhances the interaction between different atoms, indicating that the existence of impurity atoms will strongly interfere with the electronic structure of the ZnO semiconductor, which can be further verified by analyzing the splitwave state density. Compared with the energy band structure diagram of $\text{Zn}_{16}\text{O}_{16}$, the conduction band and valence band of all doped systems move towards the low energy direction. As the valence band moves down more, the Fermi energy level enters the conduction band. The combined action of the Burstein–Moss effect and the band gap contraction effect explains this phenomenon [35,36]. The La atom introduces impurity energy levels at the bottom of the conduction band and the top of the valence band. In combination with the density of states in Figure 2b,c, the impurity energy levels are mainly contributed by the electrons of La-5d and -6s states, indicating that the doping of ZnO with the La atom is a donor-type doping. The introduction of extra carriers (electrons) by the La atom enhances the conductivity and metallicity of the system and these carriers degenerate. Therefore, the La-doped ZnO systems are n-type degenerate semiconductors. The difference between the Fermi level of $\text{Zn}_{15}\text{La}_1\text{O}_{16}$ and the bottom of the conduction band is 1.48 eV, and the difference between the Fermi level of $\text{Zn}_{14}\text{La}_2\text{O}_{16}$ and the bottom of the conduction band is 1.87 eV. $\text{Zn}_{14}\text{La}_2\text{O}_{16}$ shows stronger metallicity and conductivity. The results show that the La-doped ZnO system has photoelectric transport characteristics, which can provide theoretical guidance for the experimental preparation of highly conductive ZnO thin films. In addition, the spin-up and spin-down band structures of the La-doped ZnO system are the same and no spin splitting occurs, indicating that La-doped ZnO materials do not exhibit magnetic characteristics.

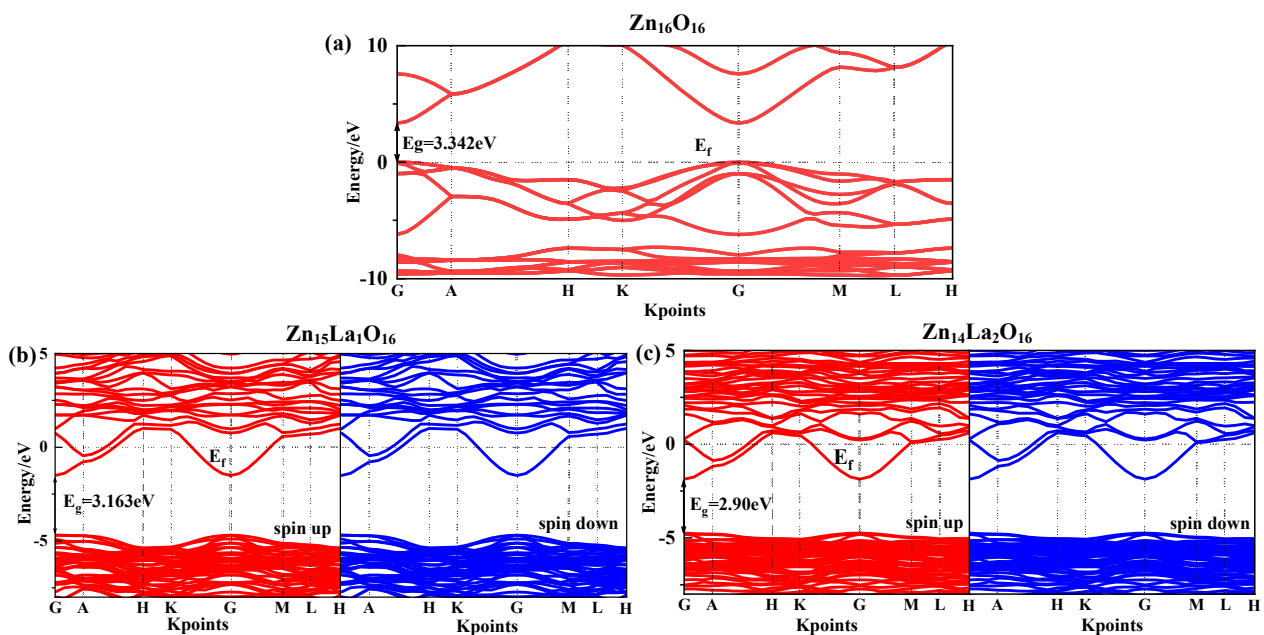


Figure 2. Energy band structure near Fermi surface. (a) $\text{Zn}_{16}\text{O}_{16}$, (b) $\text{Zn}_{15}\text{La}_1\text{O}_{16}$, (c) $\text{Zn}_{14}\text{La}_2\text{O}_{16}$. Annotation: The red lines representative spin up and the blue lines representative spin down.

3.3. Density of States Analysis

The density of the state is one of the important properties of semiconductor materials. It can scientifically explain the energy band structure, optical properties, and magnetic properties of semiconductors, and is a visual result of the energy band structure. Figure 3 shows the total density of states and partial density of states of intrinsic ZnO and La-doped ZnO systems under spin polarization conditions. Figure 3a shows the total density of states and the density of separated states of $\text{Zn}_{16}\text{O}_{16}$. Analysis shows that the GGA+U method can correct the interaction between electrons in the atomic orbits. The electronic density of the Zn-3d state and O-2p state in the valence band near the Fermi level are obviously

separated, so the valence band becomes wider and the p-d hybridization becomes weaker. In the deep valence band $-15.8\text{ eV}\sim-14.3\text{ eV}$ region, it is contributed by O-2s state electrons, and its locality is strong. In the $-10.3\text{ eV}\sim-6.9\text{ eV}$ valence band region, it is contributed by Zn-3d state electrons and some O-2p state electrons. Therefore, there is a strong pd hybridization between Zn-3d state electrons and O-2p state electrons, forming a stronger Zn-O bond. In the upper valence band $-6.3\text{ eV}\sim 0\text{ eV}$ region, it is contributed by O-2p state electrons, and in the conduction band region, it is contributed by Zn-4s and 3p state electrons. The calculations are consistent with the theoretical calculations of Li. H [37]. In addition, it is found that the Zn-4s state electrons determine the bottom position of the intrinsic ZnO conduction band, and the O-2p state electrons determine the top position of the intrinsic ZnO valence band. Therefore, when the Zn atom and the O atom bond, the electrons in the above two states interact to form a chemical bond, of which the electron in the O-2p state contributes the most [38]. In addition, the total state densities of intrinsic ZnO are completely symmetrical in spin-up and spin-down conditions, and the net spin state density is a straight line, indicating that the intrinsic ZnO is nonmagnetic.

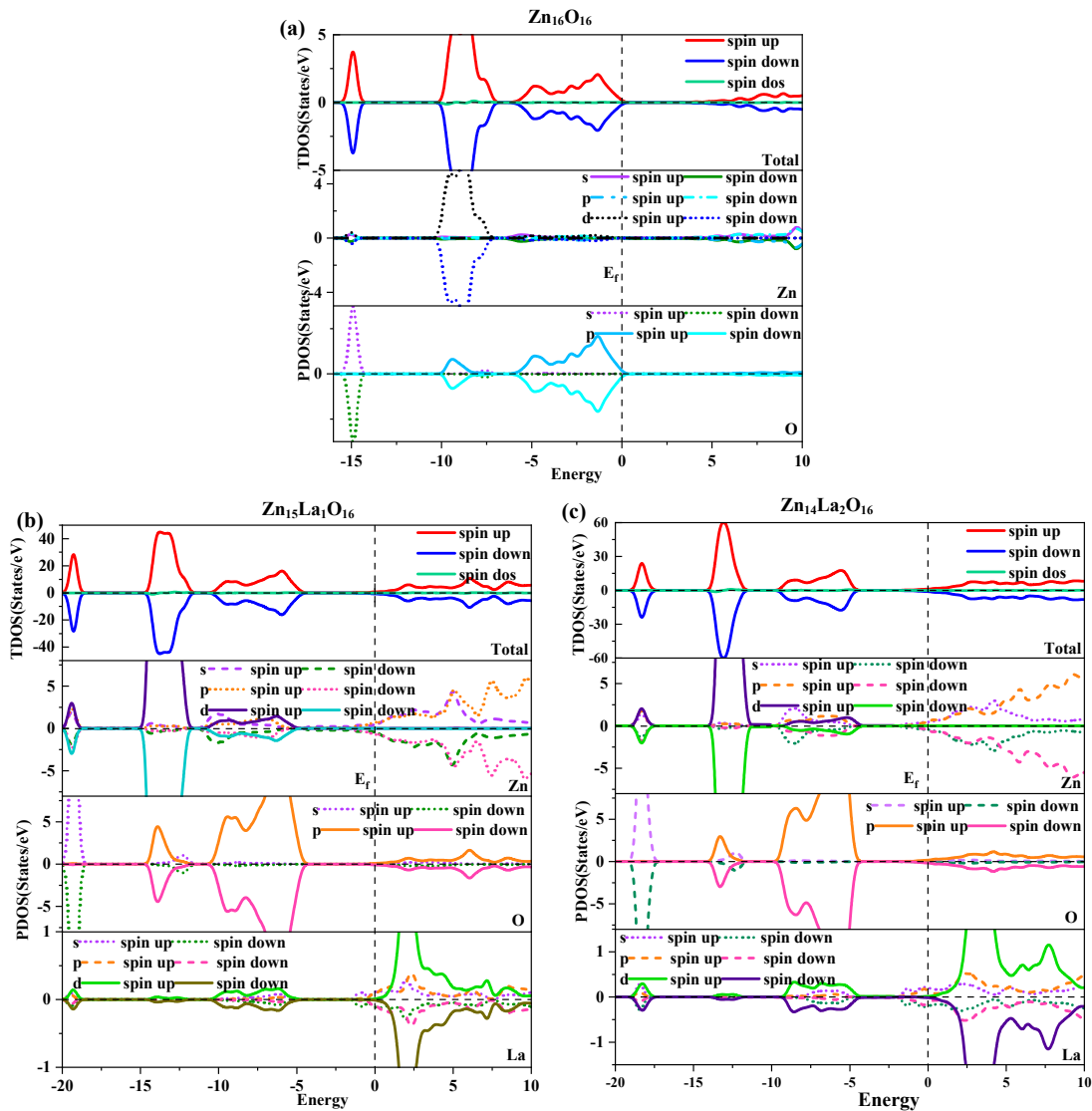


Figure 3. Density of state. (a) Zn₁₆O₁₆, (b) Zn₁₅La₁O₁₆, (c) Zn₁₄La₂O₁₆.

Figure 3b,c show the total density of states and the separate density of states of Zn₁₅La₁O₁₆ and Zn₁₄La₂O₁₆. Analysis shows that the number of conductive carriers increases due to the doping of La, which causes the conduction band and valence band

to move towards the low energy direction and the Fermi level to enter the conduction band, thereby forming a degenerate semiconductor that exhibits n-type semiconductor properties. In the doping of La atoms, the hybridization of the La-5d and La-5p state electrons has a major impact on the state of the density of the valence band top, band gap, and conduction band bottom of the doped system. The impurity energy level contributed by the La-5d state electrons at the bottom of the conduction band produces the Urbach tail effect. With the increase in the La doping concentration, the band tail moves towards the direction of low energy, and the band gap further decreases. Compared with Zn and O atoms, the partial wave state density of La accounts for a smaller proportion of the total density of states. Except that some orbital electrons have a greater impact on the local density of states, the overall effect on the performance of the doped system is small. In the $-20\text{ eV}\sim-18.7\text{ eV}$ energy region, it is mainly contributed by O-2s and Zn-3d state electrons; in the $-14.7\text{ eV}\sim-11.6\text{ eV}$ energy region, it is mainly contributed by Zn-3d and O-2p state electrons; in the $-10.4\text{ eV}\sim-4.9\text{ eV}$ energy region, it is mainly contributed by Zn-3d, O-2p, and La-5d state electrons; and the local state of the conduction band is mainly contributed by La-5d state electrons. Therefore, p-d hybridization is formed in the Zn-3d state, O-2p state, and La-5d state near the Fermi level. In addition, the total density of the state of $\text{Zn}_{15}\text{La}_1\text{O}_{16}$ and $\text{Zn}_{14}\text{La}_2\text{O}_{16}$ systems are completely symmetrical in the spin-up and spin-down conditions, and the net spin density of the state is a straight line, indicating that the La-doped ZnO system is nonmagnetic.

3.4. Orbital Charge Analysis

The Mulliken population analysis method is often cited by scholars to understand the bonding behavior of crystals [39,40]. In this work, we also used this approach to calculate the orbital charge number, which is used to describe the charge transfer after bonding. Table 2 shows the Mulliken charge distribution of intrinsic ZnO and La-doped ZnO systems under spin polarization conditions. It can be seen from the analysis that the Zn atom in $\text{Zn}_{16}\text{O}_{16}$ has a strong ability to lose electrons, with a +0.93 positive charge, and the O atom has a strong ability to obtain electrons, with a -0.93 negative charge. This is mainly due to the transfer of electrons on the Zn-4s orbital to the O-2p orbital. A covalent bond containing ionic bond components is formed between the Zn atom and the O atom. In addition, the spin-up and spin-down electron numbers of each orbit of Zn and O atoms are the same, indicating that the intrinsic ZnO is nonmagnetic, which is consistent with Section 3.3 on density of state analysis.

Table 2. Mulliken charge distribution of intrinsic ZnO and La-doped ZnO systems.

Model	Atom	s	p	d	Total/eV	Net Charge/e
$\text{Zn}_{16}\text{O}_{16}$	Zn (spin up)	0.20	0.34	4.99	5.54	0.93
	Zn (spin down)	0.20	0.34	4.99	5.54	-
	O (spin up)	0.92	2.55	0.00	3.46	-0.93
	O (spin down)	0.92	2.55	0.00	3.46	-
$\text{Zn}_{15}\text{La}_1\text{O}_{16}$	Zn (spin up)	0.19	0.36	4.99	5.54	0.93
	Zn (spin down)	0.19	0.36	4.99	5.54	-
	O (spin up)	0.91	2.56	0.00	3.47	-0.95
	O (spin down)	0.91	2.56	0.00	3.47	-
	La (spin up)	0.15	-0.22	0.68	0.62	1.77
	La (spin down)	0.15	-0.22	0.68	0.62	-
$\text{Zn}_{14}\text{La}_2\text{O}_{16}$	Zn (spin up)	0.26	0.36	5.00	5.62	0.76
	Zn (spin down)	0.26	0.36	5.00	5.62	-
	O (spin up)	0.93	2.53	0.00	3.46	-0.92
	O (spin down)	0.93	2.53	0.00	3.46	-
	La (spin up)	0.25	-0.17	0.71	0.79	1.42
	La (spin down)	0.25	-0.17	0.71	0.79	-

In doping the ZnO system with the La atom, the doped atom loses electrons and becomes a positively charged center with the characteristics of donor impurities. In the

$Zn_{15}La_1O_{16}$ system, the La atom has a positive charge of +1.77, the Zn atom has a positive charge of +0.93 when it loses electrons, and the O atom has a negative charge of -0.95 when it gains electrons. This is mainly due to the transfer of electrons on the 6s orbital of the La atom to the 2p orbital of the O atom. In the $Zn_{14}La_2O_{16}$ system, the La atom has a positive charge of +1.42 when it loses fewer electrons, the Zn atom has a positive charge of +0.83 when it loses fewer electrons, and the O atom has a negative charge of -0.91 when it obtains fewer electrons. The charge distribution of the O-2s and -2p orbitals changes little after La doping, indicating that stable chemical bonds can be formed between the O atoms and La atoms. In addition, because the valence electrons of the La atom and the Zn atom are different, the La atom has more positive charges, indicating that the La atom contributes more electrons. These results can also be described by NBO methods, which will be used to further analyze the orbital charge in a future study. It is also found that the charge numbers of $Zn_{15}La_1O_{16}$ and $Zn_{14}La_2O_{16}$ systems are identical on spin-up and spin-down orbitals, indicating that the La-doped ZnO system has no magnetism, which is consistent with density of state analysis in Section 3.3.

3.5. Analysis of Population Value and Bond Length

In order to more intuitively show the distribution of charge in the intrinsic ZnO and La-doped ZnO systems, the population value and bond length of the doped system are calculated, and the calculation results are listed in Table 3. The size of the population value can intuitively reflect the strength of covalent bonds and ionic bonds. Generally, the zero value of the chemical bond population represents the ideal ionic bond. A positive bond population indicates that atoms are bonded, and a high value indicates that bonds are covalent bonds. The larger the population value, the stronger the covalent bonds. A low value indicates that atoms are interacting with ions. The smaller the population value, the stronger the ionic bond. A negative bond population indicates that there is antibond between atoms, that is, there is no bond [41,42]. By analyzing the Zn-O bond between other Zn and O atoms in the system that are not directly connected with the doped La atom, we found that, after doping, the population value of the Zn-O_{max} bond decreases gradually and the bond length increases gradually, indicating that its covalence gradually weakens. In addition, the population value of the La-O bond is lower than that of the Zn-O bond. This is because the electronegativity of La (1.10) is lower than that of Zn (1.65), which makes it easier for O atoms to obtain electrons from La atoms during bonding. As a result, the polarity of the La-O bond is stronger. With the increase in the La doping concentration, there are some changes to the population values of La-O bonds parallel to the c-axis and La-O bonds perpendicular to the c-axis change. This is due to the increased mutual repulsion between excess positive charges after replacing Zn²⁺ with La³⁺, and the reduced hybridization between La³⁺ and O²⁻ ions. The results show that with the increase in La doping, the overlap of the electron cloud around the La-O bond decreases, which leads to decreased covalence and enhanced ionic property.

Table 3. Population value and bond length of inherent ZnO and La-doped ZnO system.

Model	Bond Type	Population Value	Bond Length
$Zn_{16}O_{16}$	Zn-O _{max}	1.08	1.966
	Zn-O _{min}	0.12	1.975
$Zn_{15}La_1O_{16}$	Zn-O _{max}	0.32	2.052
	Zn-O _{min}	0.41	1.966
	La-O (//c)	0.27	2.313
	La-O (⊥c)	0.3	2.264
$Zn_{14}La_2O_{16}$	Zn-O _{max}	0.25	2.166
	Zn-O _{min}	0.39	2.050
	La-O (//c)	0.27	2.303
	La-O (⊥c)	0.18	2.376

3.6. Analysis of Differential Charge Density

By analyzing the differential charge density diagram of ZnO before and after doping, the bonding between atoms in the La-doped ZnO system can be discussed in a more vivid and intuitive manner [43,44]. The differential charge density distributions of $\text{Zn}_{16}\text{O}_{16}$, $\text{Zn}_{15}\text{La}_1\text{O}_{16}$, and $\text{Zn}_{14}\text{La}_2\text{O}_{16}$ on the plane of the doped La atom under spin polarization conditions are calculated, and the calculation results are shown in Figure 4. In the figure, the green electron cloud represents electron aggregation, the pink electron cloud represents electron dissipation, the red color scale bar represents electron gain, and the blue color scale represents electron loss. The darker the color is, the more electrons are transferred. It can be seen from the analysis that, compared with the electron cloud between the Zn atom and O atom in the intrinsic ZnO system, the doped La atom has a greater impact on the electron cloud density of the surrounding O atom, the interaction is enhanced, and the directivity of the electron cloud is strong. Most of the electrons lost in La are transferred to the O atom. With the increase in the doping concentration of the La atoms, the electron transfer density in the La-O bond area increases, but the overlap of the electron cloud between the La atom and the surrounding O atom in the doped system is weakened. The covalent bond of the doped system is weakened, while the ionic bond of the doped system is strengthened. The calculated results are consistent with the population value, bond length, and stability analysis results of the doped system. These results also can be described by NBO methods, which will be used to further analyze the orbital charge in the future study.

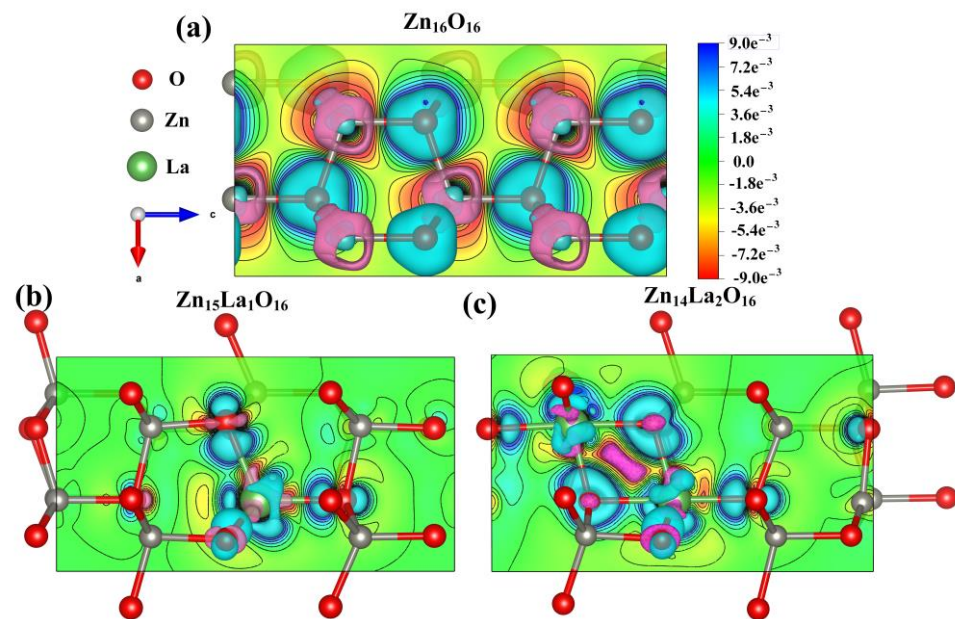


Figure 4. Differential charge density diagram. (a) $\text{Zn}_{16}\text{O}_{16}$, (b) $\text{Zn}_{15}\text{La}_1\text{O}_{16}$, (c) $\text{Zn}_{14}\text{La}_2\text{O}_{16}$.

3.7. Optical Properties

The optical properties of semiconductors are closely related to the electronic structure. In the linear response range, the research on the macroscopic optical properties of solids is generally based on the research on the $\varepsilon(\omega) = \varepsilon_1(\omega) + i\varepsilon_2(\omega)$ of the complex dielectric function,

$$\varepsilon_1 = n^2 - \kappa^2 \quad (2)$$

$$\varepsilon_2 = 2n\kappa \quad (3)$$

where n is refractive index and κ is extinction coefficient.

Electronic transition includes the in-band transition and inter-band transition of electrons: the in-band transition mainly occurs in metals and the inter-band transition mainly exists in semiconductors. The inter-band transition can be further divided into direct

transition and indirect transition. The indirect transition involves phonon dispersion, which has little effect on the dielectric function, so it can be ignored. In this paper, the optical properties of ZnO doped systems are systematically analyzed by calculating its dielectric function, absorption coefficient, reflectivity, and energy loss function. According to the definition of direct transition probability and Kramers–Kronig dispersion relation, the imaginary part $\varepsilon_2(\omega)$ and real part $\varepsilon_1(\omega)$ of the crystal dielectric function, absorption coefficient, reflectivity, and energy loss function can be deduced. The specific deduction process will not be repeated [45–47].

$$\varepsilon_2(\omega) = \frac{\pi}{\varepsilon_0} \left(\frac{e}{m\omega} \right)^2 \cdot \sum_{V,C} \left\{ \int_{BZ} \frac{2d\vec{K}}{(2\pi)^3} \left| \vec{a} \cdot \vec{M}_{V,C} \right|^2 \delta \left[E_C(\vec{K}) - E_V(\vec{K}) - \hbar\omega \right] \right\} \quad (4)$$

$$\varepsilon_1(\omega) = 1 + \frac{2e}{\varepsilon_0 m^2} \cdot \sum_{V,C} \int_{BZ} \frac{2d\vec{K}}{(2\pi)^3} \frac{\left| \vec{a} \cdot \vec{M}_{V,C}(\vec{K}) \right|^2}{\left[E_C(\vec{K}) - E_V(\vec{K}) \right] / \hbar} \cdot \frac{1}{\left[E_C(\vec{K}) - E_V(\vec{K}) \right]^2 / \hbar^2 - \omega^2} \quad (5)$$

$$R(\omega) = \frac{(n-1)^2 + k^2}{(n+1)^2 + k^2} \quad (6)$$

$$\alpha \equiv \frac{2\omega\kappa}{c} = \frac{4\pi\kappa}{\lambda_0} \quad (7)$$

$$L(\omega) = \text{Im} \left(\frac{-1}{\varepsilon(\omega)} \right) - \frac{\varepsilon_2(\omega)}{[\varepsilon_1^2(\omega) + \varepsilon_2^2(\omega)]} \quad (8)$$

where ε_0 is the dielectric constant in vacuum, λ_0 is the wavelength in vacuum, \hbar is Planck's constant, C and V are the conduction band and valence band, respectively, BZ is the first Brillouin zone, \vec{K} is the electron wave vector, a is the unit direction vector of the vector potential A , $M_{V,C}$ is the transition matrix element, ω is the electromagnetic wave frequency, $E_C(K)$ and $E_V(K)$ are the intrinsic energy level on the conduction band and the valence band, respectively, $R(\omega)$ is the reflectivity, α is the absorption coefficient, and $L(\omega)$ is the energy loss function.

The size of the dielectric constant indicates the capacity of the medium to bind charges. The larger the dielectric constant is, the stronger the capacity of the medium to bind charges is. On the contrary, it means that the binding capacity is weaker [48]. The real part of the dielectric function represents the change in the dielectric constant with the change in photoelectron energy [49], and the imaginary part of the dielectric function reflects the information between the energy band structure and the optical transition. Figure 5 shows the dielectric function curve of the intrinsic ZnO and La-doped ZnO systems. The photoelectron lifetime τ_c on the conduction band is proportional to the dielectric constant ε_1 of the photocatalyst. Therefore, the larger the ε_1 of the system, the larger the τ_c , that is, the longer the photoelectron lifetime on the conduction band [11]. Figure 5a shows the real part curve of the dielectric function. It can be seen from the analysis that the average static dielectric constant $\varepsilon_1^{ave}(0)$ of $\text{Zn}_{16}\text{O}_{16}$ is 3.21, and the average static dielectric constant $\varepsilon_1^{ave}(0)$ of $\text{Zn}_{15}\text{La}_1\text{O}_{16}$ and $\text{Zn}_{14}\text{La}_2\text{O}_{16}$ is 3.21 and 4.66, respectively. With the increase in the La doping concentration, the dielectric constant of the doped system becomes larger, indicating that La enhances the polarization of the doped system and has strong binding capacity to electrons, that is, it extends the photoelectron lifetime on the conduction band of the doped system and brings good conductivity.

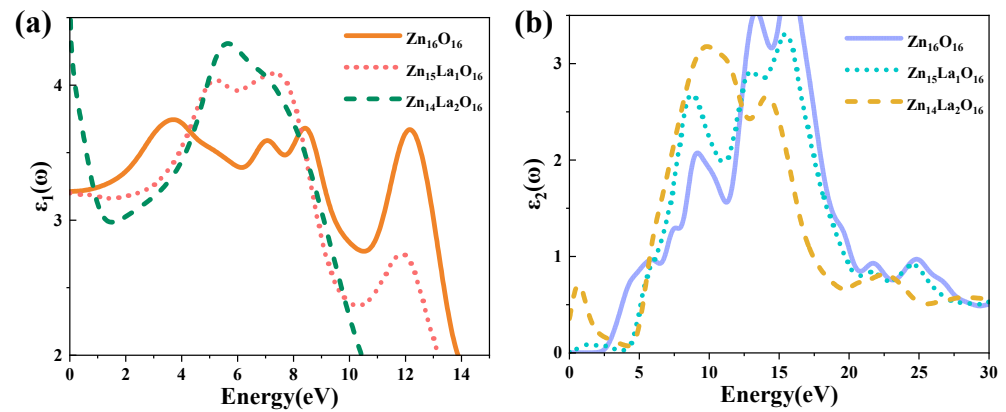


Figure 5. Dielectric function. (a) Real part of dielectric function, (b) imaginary part of dielectric function.

Figure 5b shows the imaginary part curve of the dielectric function. It can be seen from the analysis that the $\varepsilon_2(\omega)$ of the imaginary part of the dielectric function of the intrinsic ZnO mainly has four peaks: the first dielectric peak is located at 5.82 eV, which is mainly formed by the electronic transition from the top of the valence band to the energy band near the bottom of the conduction band, that is, the transition from the O-2p state at the top of the valence band to the Zn-3p state at the bottom of the conduction band. The second dielectric peak is located at 9.15 eV, which is mainly formed by the complex electronic transitions between the valence band and the top of the valence band away from the Fermi surface, that is, the transition from the Zn-3d state in the valence band to the O-2p state, the transition from the O-2s state in the valence band to the Zn-3d state and other complex electronic transitions. The third dielectric peak is located at 13.33 eV, which is mainly formed by the complex electronic transition between the valence band and the bottom of the conduction band away from the Fermi surface, that is, the transition from the Zn-3d state in the valence band to the Zn-3p state at the bottom of the conduction band. The fourth dielectric peak is located at 15.71 eV, which is mainly formed by the complex electronic transition between the valence band and the bottom of the conduction band away from the Fermi surface, that is, the transition from the O-2s state in the valence band to the Zn-3p state at the bottom of the conduction band. The $\text{Zn}_{14}\text{La}_2\text{O}_{16}$ system has a new peak near 0.67 eV, which is small, and is caused by the in-band transition of La-5d orbital electrons. However, this peak is not found in the imaginary part of the dielectric function of $\text{Zn}_{15}\text{La}_1\text{O}_{16}$ system. In addition, the doping of La affects the O-2s state electrons in the deep valence band region. As a result, with the increase in the doping amount of La, the peak near 9.09 eV moves to the high energy direction and the peak intensity is enhanced, while the peak near 15.71 eV moves to the low energy direction and the peak intensity is weakened.

Figure 6 shows the absorption spectrum and reflection spectrum of the intrinsic ZnO and La-doped ZnO system. Optical absorption is one of the most essential optical properties of ZnO semiconductor materials, reflecting the luminescence mechanism of the spectrum generated by the electronic transition between energy levels. The absorption spectrum calculated according to Formulas (1)–(7) is shown in Figure 6a, with an absorption coefficient of 10^5 cm^{-1} . Analysis shows that the intensity of the first peak of the doped system is not high, and is generally located in the lower energy range. It is generated due to the electrons that absorb energy and transition from the top of the valence band to the conduction band. Though not obvious, the first peak is crucial. The optical absorption edge of the intrinsic ZnO is around 3.30 eV. The absorption edge is where intrinsic absorption begins to appear and intrinsic absorption determines the key optical properties of ZnO. With the increase in photon energy, the absorption coefficient increases sharply in the order of 10^5 and strong light absorption occurs, indicating that the direct transition begins. In the visible light region (1.64 eV~3.19 eV), the light absorption edge of $\text{Zn}_{15}\text{La}_1\text{O}_{16}$ and

$\text{Zn}_{14}\text{La}_2\text{O}_{16}$ moves towards the direction of high energy, which causes a blue shift. The widening of the optical bandgap E_g because of La atoms introduce a large number of carriers (electrons) as donor atoms, Fermi levels enter the conduction band, resulting in the Burstein–Moss effect. This maximal widening is almost equal to the reported value 0.38 eV resulted from La doping of 0.14 at.%, and larger than the reported value 0.2 and 0.13 eV resulted from La doping of 0.3–0.57 at.% [24]. The optical absorption spectra of $\text{Zn}_{15}\text{La}_1\text{O}_{16}$ and $\text{Zn}_{14}\text{La}_2\text{O}_{16}$ show a smaller new absorption peak near 1.06 eV, which is caused by the in-band transition of La-5d orbit. In the visible light region, compared with the intrinsic ZnO, as the doping concentration of La increases, the absorption spectrum moves to the direction of high energy, resulting in a blue shift, and decreased light absorption intensity. The main absorption peak of $\text{Zn}_{16}\text{O}_{16}$ is at 16.96 eV, the main absorption peak of $\text{Zn}_{15}\text{La}_1\text{O}_{16}$ is at 16.60 eV, and the main absorption peak of $\text{Zn}_{14}\text{La}_2\text{O}_{16}$ is at 15.38 eV, which is in the vacuum ultraviolet region. With the increase in La doping concentration, the absorption peak moves to the direction of low energy, resulting in a red shift and a decreased intensity of the main absorption peak. As the doping of La introduces new impurity energy levels, a new emission center is developed, leading to the red shift of ultraviolet emission. These results are the same as the reported conclusion that the light absorption of the films in UV range first blue-shift and then red-shift with the increase in the La content (0.5–2.0 at.%) [30]. The absorption peak mainly comes from the transition of excited state electrons from the valence band to the conduction band. The weakening of the absorption peak intensity indicates that the transition process of electrons in this excited state is reduced after La doping. In addition, the absorption peaks near 25.35 eV, 34.58 eV, and 38.86 eV are red-shifted and weaker than $\text{Zn}_{16}\text{O}_{16}$. Therefore, the optical properties of La-doped ZnO become worse in the visible light range, but the light absorption in the ultraviolet region is good, so it can be used as a short wave device.

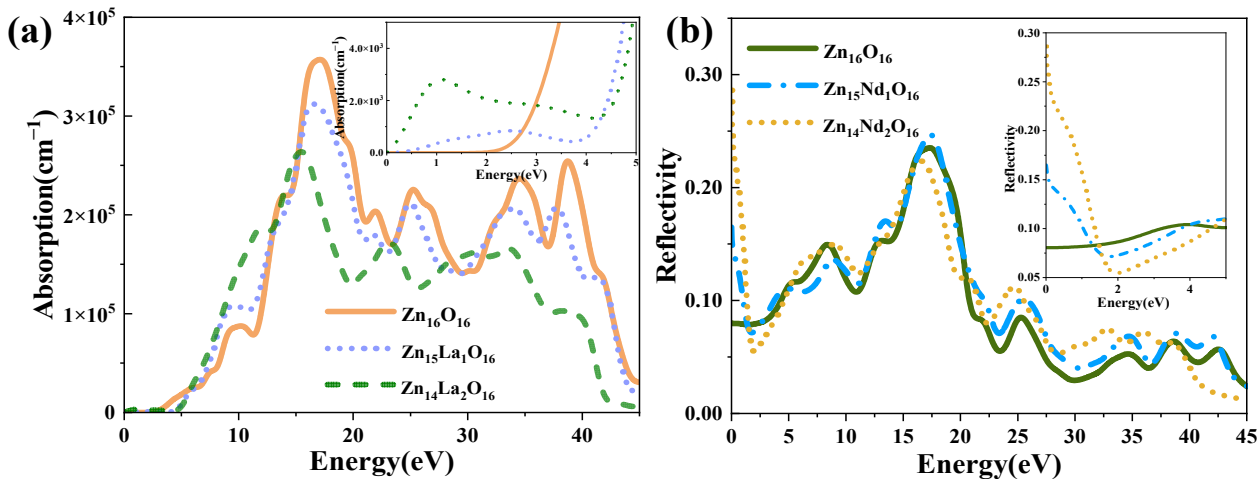


Figure 6. (a) Absorption spectrum, (b) Reflectivity.

Reflectivity refers to the macroscopic phenomenon of the electron transition between energy bands in solids under the interference of a photoelectric magnetic field. The reflectivity of intrinsic ZnO and La-doped ZnO systems calculated according to Formulas (1)–(6) is shown in Figure 6b. The static reflectivity $R(0)$ of $\text{Zn}_{16}\text{O}_{16}$ is 0.08, and that of $\text{Zn}_{15}\text{La}_1\text{O}_{16}$ and $\text{Zn}_{14}\text{La}_2\text{O}_{16}$ is 0.08 and 0.14. It has high reflectivity in the range of 16 eV to 20 eV. $\text{Zn}_{16}\text{O}_{16}$ has maximum reflectivity of 0.24 at 17.2 eV, $\text{Zn}_{15}\text{La}_1\text{O}_{16}$ has maximum reflectivity of 0.28 at 17.8 eV, and $\text{Zn}_{14}\text{La}_2\text{O}_{16}$ has maximum reflectivity of 0.23 at 16.0 eV. In the visible light area, with the increase in the La doping concentration, the reflectivity decreases, which is lower than the intrinsic ZnO. When photons pass through the material, some of them will be reflected, some will be absorbed by the material, and the rest will be transmitted from the material. Therefore, the absorption coefficient and reflectivity of La-doped ZnO decrease both in the visible and ultraviolet regions, thereby resulting in increased transmittance.

Photoconductivity indicates the change in the conductivity of semiconductor materials along with the light intensity. Figure 7a shows the photoconductivity of intrinsic ZnO and La-doped ZnO systems, which strictly corresponds to the imaginary part $\epsilon_2(\omega)$ of the dielectric function (Figure 5b). The analysis shows that the intrinsic ZnO and La-doped ZnO systems have high conductivity, in the range of 10 eV to 20 eV, and the real part reaches its main peak near 15 eV of energy. The peak value of intrinsic ZnO is 7.71 fs^{-1} , and the peak values of $\text{Zn}_{15}\text{La}_1\text{O}_{16}$ and $\text{Zn}_{14}\text{La}_2\text{O}_{16}$ are 6.21 fs^{-1} and 4.59 fs^{-1} . In the visible light region, the photoconductivity of the intrinsic ZnO and La-doped ZnO systems increases with the increase in the incident photon energy. Compared with the photoconductivity value in the low energy region, it is found that the photoconductivity of the La-doped ZnO system is greater than that of the intrinsic ZnO. This is due to the introduction of excess carriers by the La atom at the Fermi level of the doped system, which increases the photoconductivity in the low energy region, but the photoconductivity of all systems is small. This shows that the doping of La improves the photoconductivity of the ZnO semiconductor in the visible light region.

The energy loss function describes the energy loss of electrons passing through a homogeneous crystal, and its peak value is related to the plasma frequency. Based on calculations with Formulas (1)–(8), the energy loss function reflects the energy loss when photons pass through the crystal. Figure 7b is the energy loss function of the intrinsic ZnO and La-doped ZnO systems. Analysis shows that the plasma frequency of $\text{Zn}_{16}\text{O}_{16}$ is 40.29 eV, the plasma frequency of $\text{Zn}_{15}\text{La}_1\text{O}_{16}$ is 38.79 eV, and the plasma frequency of $\text{Zn}_{14}\text{La}_2\text{O}_{16}$ is 18.57 eV. With the increase in the La doping amount, the peak value is red-shifted, and the intensity is always weaker than the intrinsic ZnO system.

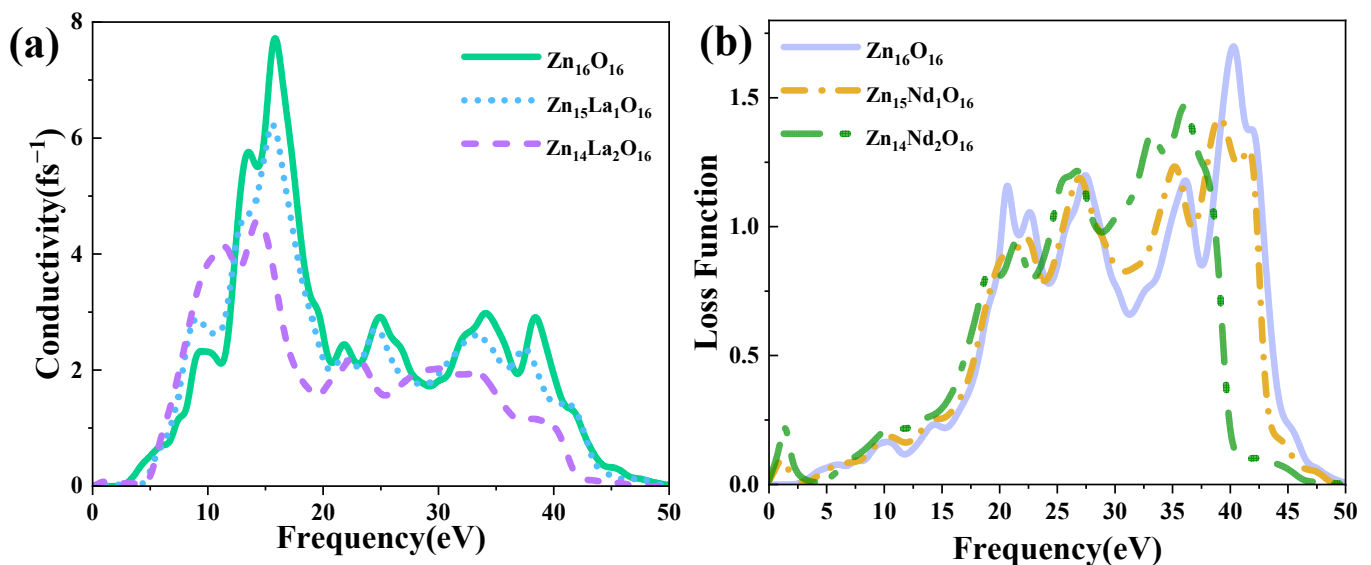


Figure 7. (a) Photoconductivity, (b) Energy loss function.

3.8. Magnetic Properties

At present, according to the research progress of ZnO thin magnetic semiconductors, the magnetic properties of ZnO semiconductors are induced by intrinsic defects, 3d transition metals, rare-earth elements, and other magnetic ions doping and non-magnetic ions doping. For doping, 3d transition elements (Cr, Mn, Fe, and Co) are the preferred elements due to their unpaired electrons in the 3d shell and large magnetic moment, which can produce strong magnetic properties. A large number of studies have shown that effective transition metal doping can improve the photocatalytic performance of ZnO while presenting room temperature ferromagnetism [28,50,51]. In addition, the optical and magnetic properties of the over metal-doped ZnO system are closely related to the transition metal doping type, preparation environment, and annealing environment. However, the

magneto-optical properties of rare-earth-doped ZnO mainly depend on the interaction between the 4f electrons of rare-earth-doped elements and the defects arising from doping in the ZnO body. The magnetic and optical properties of rare-earth doped ZnO have attracted the attention of many researchers [52–54]. This paper adopts the spin polarization calculation method. The calculation results output values of $2 \times \int \text{Integrated Spin Density}$ and $2 \times \int |\text{Spin Density}|$. The former represents the spin polarization DOS integral results, that is $\sum M$, the difference between spin-up and spin-down conditions. This result is the Bohr magnetic moment of the system, and 2 is the spin magnetic moment g factor. Whereas, the latter represents the sum of the absolute spin polarization DOS integral, that is $\sum |M|$, the sum of spin-up and spin-down electron density of state integrals. These two values can be used to preliminarily judge the magnetism of the system. The $\sum M = 0$, $\sum |M| = 0$ of $\text{Zn}_{15}\text{La}_1\text{O}_{16}$ and $\text{Zn}_{14}\text{La}_2\text{O}_{16}$, the total magnetic moment is 0. At the same time, by analyzing the density of states in Figure 3, it is found that the total density of states and the partial wave density of states in the $\text{Zn}_{15}\text{La}_1\text{O}_{16}$ and $\text{Zn}_{14}\text{La}_2\text{O}_{16}$ systems are completely symmetrical in spin-up and spin-down conditions, and the net spin density of states is also a straight line, indicating that the La-doped ZnO system is nonmagnetic. The analysis of the Mulliken orbital charge distribution in Table 2 shows that, in the $\text{Zn}_{15}\text{La}_1\text{O}_{16}$ and $\text{Zn}_{14}\text{La}_2\text{O}_{16}$ systems, the spin-up and spin-down orbital electron number of each atom are identical, indicating that the La-doped ZnO system is nonmagnetic, so the La-doped ZnO system has no magnetic moment and no magnetism, which is consistent with the calculation results in study [11], while [55] holds that La-doped ZnO in replacement of Zn is magnetic. The authors of [56] proved that it was due to the existence of Zn vacancies in the doped system.

4. Conclusions

In this paper, based on the density functional theory, the GGA+U method is used to calculate the effect of rare-earth element La doping at different concentrations on the electronic structure, optical properties, and magnetic properties of ZnO under spin polarization conditions. The electronic structure calculation results show that the cell of the La-doped ZnO system is distorted, and the formation energy is less than zero, in which case it is easy to dope. After La doping, the band gap narrows, the Fermi level enters the conduction band, and the excess carriers introduced by La atoms degenerate. The La-doped ZnO system is an n-type degenerate semiconductor, and the carriers enhance the conductivity and metallicity of the system. The calculation results for optical properties show that in the visible light region, the optical absorption edge of the La-doped ZnO system experiences a blue shift, which increases the average static dielectric constant and strengthens the polarization ability and the capacity to bind charges. The photoconductivity of the doped ZnO system is improved. The calculation results on magnetic properties suggest that the magnetic moment of La-doped ZnO system is 0, and the system has no magnetism.

Author Contributions: F.Z. and S.X. supervised the research. Q.W. calculated a series of properties of the material and wrote the first draft. B.Z., G.L., J.N. and T.S. analyzed the data and revised the paper. All authors have read and agreed to the published version of the manuscript.

Funding: This research was funded by the National Natural Science Foundation of China (No. 62264015), the National Science Foundation of Shaanxi Province, China (2021JQ-635), Scientific Research Program of Yan'an University (YDQ2020-08) and Scientific and Technological Innovation Team (2017CXTD-01).

Data Availability Statement: All data are presented in the form of charts in the article.

Conflicts of Interest: The authors declare no conflict of interest.

References

1. Djuricic, A.B.; Ng, A.; Chen, X.Y. ZnO nanostructures for optoelectronics: material properties and device applications. *Prog. Quantum Electron.* **2010**, *34*, 191–259. [\[CrossRef\]](#)
2. Tirumalareddygar, S.R.; Guddeti, P.R.; Ramakrishna Reddy, K.T. A critical study of the optical and electrical properties of transparent and conductive Mo-doped ZnO films by adjustment of Mo concentration. *Appl. Surf. Sci.* **2018**, *458*, 333–343. [\[CrossRef\]](#)
3. Tay, Y.Y.; Tan, T.T.; Li, S. Determinants of the structured and structureless green emissions of ZnO. *Solid State Commun.* **2011**, *151*, 372–376. [\[CrossRef\]](#)
4. Ozgur, U.; Alivov, Y.I.; Liu, C.; Teke, A.; Reshchikov, M.; Dogan, S.; Avrutin, V.; Cho, S.; Morkoc, H. A comprehensive review of ZnO materials and devices. *J. Appl. Phys.* **2005**, *98*, 41301. [\[CrossRef\]](#)
5. Santosh, S.; Gupta, K.; Sudarshan, R. Optical nanomaterials with focus on rare earth doped oxide: A Review. *Mater. Today Commun.* **2021**, *27*, 102277.
6. Li, H.; Li, W.; Gu, S.; Wang, F.; Zhou, H. In-built Tb⁴⁺/Tb³⁺ redox centers in terbium-doped bismuth molybdate nanoglass for enhanced photo catalytic activity. *Catal. Sci. Technol.* **2016**, *6*, 3510–3519. [\[CrossRef\]](#)
7. Li, Y.; Wang, R.; Zheng, W.; Li, Y. Silica-coated Ga (III)-doped ZnO: Yb³⁺, Tm³⁺ upconversion nanoparticles for high-resolution in vivo bioimaging using near infrared to near-infrared upconversion emission. *Inorg. Chem.* **2019**, *58*, 8230–8236. [\[CrossRef\]](#)
8. Yao, N.; Huang, J.; Fu, K.; Deng, X.; Ding, M.; Xu, X. Rare earth ions doped phosphors for dye-sensitized solar cells applications. *RSC Adv.* **2016**, *6*, 17546–17559. [\[CrossRef\]](#)
9. Vettumperumal, R.; Kalyanaraman, S.; Thangavel, R. Optical constants and near infrared emission of Er doped ZnO sol-gel thin films. *J. Lumin.* **2015**, *158*, 493–500. [\[CrossRef\]](#)
10. Khuili, M.; Fazouan, N.; Abou El Makarim, H.; Atmani, E.; Rai, D.; Houmad, M. First-principles calculations of rare earth (RE=Tm, Yb, Ce) doped ZnO: Structural, optoelectronic, magnetic, and electrical properties. *Vacuum* **2020**, *181*, 109603. [\[CrossRef\]](#)
11. Zhang, X.J.; Mi, B.W.; Wang, X.C.; Bai, H.L. First-principles prediction of electronic structure and magnetic ordering of rare-earth metals doped ZnO. *J. Alloys Compd.* **2014**, *617*, 828–833. [\[CrossRef\]](#)
12. Reed, A.E.; Weinstock, R.B.; Weinhold, F. Natural population analysis. *J. Chem. Phys.* **1985**, *83*, 735–746. [\[CrossRef\]](#)
13. Segall, M.D.; Shah, R.; Pickard, C.J.; Payne, M. Population analysis in plane wave electronic structure calculations. *Mol. Phys.* **1996**, *89*, 571–577.
14. Hirshfeld, F.L. Bonded-atom fragments for describing molecular charge densities. *Chim. Acta* **1977**, *44*, 129–138. [\[CrossRef\]](#)
15. Glendening, E.D.; Landis, C.R.; Weinhold, F. Natural bond orbital methods. *Wiley Interdiscip. Rev. Comput. Mol. Sci.* **2011**, *2*, 1–42. [\[CrossRef\]](#)
16. Kavitha, E.; Sundaraganesan, N.; Sebastian, S.; Kurt, M. Molecular structure, anharmonic vibrational frequencies and NBO analysis of naphthalene acetic acid by density functional theory calculations. *Spectrochim. Acta Part Mol. Biomol. Spectrosc.* **2010**, *77*, 612–619. [\[CrossRef\]](#)
17. James, C.; Raj, A.A.; Reghunathan, R.; Jayakumar, V.S.; Joe, I.H. Structural conformation and vibrational spectroscopic studies of 2,6-bis(p-N,N-dimethyl benzylidene)cyclohexanone using density functional theory. *J. Raman Spectrosc.* **2006**, *37*, 1381–1392. [\[CrossRef\]](#)
18. Mouras, R.; Fontana, M.D.; Bourson, P.; Postnikov, A.V. Lattice site of Mg ion in LiNbO₃ crystal determined by raman spectroscopy. *J. Phys. Condens. Matter* **2000**, *12*, 5053–5059. [\[CrossRef\]](#)
19. Anisimov, V.I.; Zaanen, J.; Andersen, O.K. Band theory and mott insulators: Hubbard U instead of stoner I. *Phys. Rev. Condens. Matter* **1991**, *44*, 943–954. [\[CrossRef\]](#) [\[PubMed\]](#)
20. Segall, M.D.; Lindan, P.J. D.; Probert, M.J.; Pickard, C.J.; Hasnip, P.J.; Clark, S.J.; Payne, M.C. First-principles simulation: Ideas, illustrations and the CASTEP code. *J. Phys. Condens. Matter* **2002**, *14*, 2717–2744. [\[CrossRef\]](#)
21. Freysoldt, C.; Grabowski, B.; Hickel, T.; Neugebauer, J.; Kresse, G.; Janotti, A.; Van de Walle, C.G. First-principles calculations for point defects in solids. *Rev. Mod. Phys.* **2014**, *86*, 253–305. [\[CrossRef\]](#)
22. Pham, A.; Assadi, M.H.N.; Yu, A.B.; Li, S. Critical role of Fock exchange in characterizing dopant geometry and magnetic interaction in magnetic semiconductors. *Phys. Rev.* **2014**, *89*, 155110. [\[CrossRef\]](#)
23. Cococcioni, M.; de Gironcoli, S. Linear response approach to the calculation of the effective interaction parameters in the LDA+U method. *Phys. Rev.* **2005**, *71*, 035105. [\[CrossRef\]](#)
24. Ma, X.; Wu, Y.; Lv, Y. Correlation effects on lattice relaxation and electronic structure of ZnO within the GGA+U formalism. *J. Phys. Chem.* **2013**, *117*, 26029–26039.
25. Iyi, N.; Kitamura, K.; Izumi, F.; Yamamoto, J.K.; Hayashi, T.; Asano, H.; Kimura, S. Comparative study of defect structures in lithium niobate with different compositions. *J. Solid State Chem.* **1992**, *101*, 340–352. [\[CrossRef\]](#)
26. Li, F.; Zhang, C.; Zhao, M. Magnetic and optical properties of Cu-doped ZnO nanosheet: First-principles calculations. *Phys. Low-Dimens. Syst. Nanostr.* **2013**, *53*, 101–105. [\[CrossRef\]](#)
27. Sousa, S.F.; Fernandes, P.A.; Ramos, M.J. General performance of density functionals. *J. Phys. Chem.* **2007**, *111*, 10439–10452. [\[CrossRef\]](#) [\[PubMed\]](#)
28. Assadi, M.H.N.; Zhang, Y.B.; Li, S. Predominant role of defects in magnetic interactions in codoped ZnO:Co. *J. Phys. Condens. Matter* **2010**, *22*, 296004. [\[CrossRef\]](#)

29. Shakir, M.; Faraz, M.; Sherwani, M.A.; Al-Resayes, S.I. Photocatalytic degradation of the paracetamol drug using lanthanum doped ZnO nanoparticles and their in-vitro cytotoxicity assay. *J. Lumin.* **2016**, *176*, 159–167. [[CrossRef](#)]
30. He, H.Y.; Huang, J.F.; Fei, J.; Lu, J. La-doping content effect on the optical and electrical properties of La-doped ZnO thin films. *J. Mater. Sci. Mater. Electron.* **2015**, *26*, 1205–1211. [[CrossRef](#)]
31. Phuruangrat, A.; Dumrongrojthanath, P.; Yayapao, O.; Arin, J.; Thongtem, S.; Thongtem, T. Photocatalytic activity of La-doped ZnO nanostructure materials synthesized by sonochemical method. *Rare Met.* **2016**, *5*, 390–395. [[CrossRef](#)]
32. Ma, X.; Miao, L.; Bie, S.; Jiang, J. Synergistic effect of V/N-codoped anatase TiO₂ photocatalysts. *Solid State Commun.* **2010**, *150*, 689–692. [[CrossRef](#)]
33. Long, R.; English, N.J. First-principles calculation of nitrogen-tungsten codoping effects on the band structure of anatase-titania. *Appl. Phys. Lett.* **2009**, *94*, 132102. [[CrossRef](#)]
34. Bomila, R.; Srinivasan, S.; Gunasekaran, S.; Manikandan, A. Enhanced photocatalytic degradation of methylene blue dye, opto-magnetic and antibacterial behaviour of pure and La-doped ZnO nanoparticles. *J. Supercond. Nov. Magn.* **2018**, *31*, 855–864. [[CrossRef](#)]
35. Lu, J.G.; Fujita, S.; Kawaharamura, T.; Nishinaka, H.; Kamada, Y.; Ohshima, T.; Ye, Z.Z.; Zeng, Y.J.; Zhang, Y.Z.; Zhu, L.P. Carrier concentration dependence of band gap shift in n-type ZnO: Al films. *J. Appl. Phys.* **2007**, *101*, 083705. [[CrossRef](#)]
36. Schleife, A.; Rodl, C.; Fuchs, F.; Furthmueller, J.; Bechstedt, F. Optical and energy-loss spectra of MgO, ZnO, and CdO from ab initio many-body calculations. *Phys. Rev.* **2009**, *80*, 035112. [[CrossRef](#)]
37. Li, H.; Lv, Y.; Li, J.; Yu, K. Experimental and first-principles studies of structural and optical properties of rare earth (RE=La, Er, Nd) doped ZnO. *J. Alloys Compd.* **2014**, *617*, 102–107.
38. Hu, Y.; Zeng, H.; Du, J.; Hu, Z.; Zhang, S. The structural, electrical and optical properties of Mg-doped ZnO with different interstitial Mg concentration. *Mater. Chem. Phys.* **2016**, *182*, 15–21. [[CrossRef](#)]
39. Zhang, L. *First-Principles Study on the Electronic Structure and Optical Properties of La-Doped ZnO*; North University of China: Shanxi, China, 2021.
40. Xu, G.X. *Quantum Chemistry Secondary Volume*; Science Press: Beijing, China, 2022. (In Chinese)
41. Sun, C.Q. Oxidation Electronics: Bond-Band-Barrier correlation and its applications. *Prog. Mater. Sci.* **2003**, *48*, 521–685. [[CrossRef](#)]
42. Segall, M.D.; Pickard, C.J.; Shah, R.; Payne, M.C. Population analysis in plane-wave electronic structure calculations of bulk materials. *Phys. Rev.* **1996**, *54*, 16317–16320. [[CrossRef](#)]
43. Wu, H.C.; Chen, H.H.; Zhu, Y.R. Effects of Al-impurity type on formation energy, crystal structure, electronic structure, and optical properties of ZnO by using density functional theory and the hubbard-U method. *Materials* **2016**, *9*, 647. [[PubMed](#)]
44. Sha, S.L. *First-Principles Study of Effect of Different Valence States Mo-Doping and Point Defect on the Magnetic and Optical Properties of ZnO*; Inner Mongolia University of Technology: Hohhot, China, 2021.
45. Huang, K. *Solid Physics*; Higher Education Press: Beijing, China, 2002. (In Chinese)
46. Fang, R.C. *Solid State Spectroscopy*; University of Science and Technology of China Press: Hefei, China, 2001. (In Chinese)
47. Shen, X.C. *Spectra and Optical Properties of Semiconductors*, 2nd ed.; Science Press: Beijing, China, 2002. (In Chinese)
48. Yang, R.Y.; Yan, H.X.; Xiao, Y.; Guo, Z.H. The optical properties of one-dimensional ZnO: A first-principles study. *Chem. Phys. Lett.* **2007**, *446*, 98–102. [[CrossRef](#)]
49. Zhang, X.D.; Guo, M.L.; Li, W.X.; Liu, C.L. First-principles study of electronic and optical properties in wurtzite Zn_{1-x}Cd_xO. *J. Appl. Phys.* **2008**, *103*, 063721.
50. Yoon, D.H.; Muksin, K.; Raju, S. Structural, and magnetic properties of Co-doped and Mn-doped ZnO nanocrystalline DMS prepared by the facile polyvinyl alcohol gel method. *J. Supercond. Nov. Magn.* **2017**, *30*, 203–208. [[CrossRef](#)]
51. Liu, H.; Zhang, J.M. Effect of two identical 3d transition-metal atoms M doping (M=V, Cr, Mn, Fe, Co, and Ni) on the structural, electronic, and magnetic properties of ZnO. *Phys. Status Solidi B-Basic Solid State Phys.* **2017**, *254*, 1700098. [[CrossRef](#)]
52. Zamiri, R.; Lemos, A.F.; Reblo, A.; Ahangar, H.A.; Ferreira, J.M.F. Effects of rare-earth (Er, La and Yb) doping on morphology and structure properties of ZnO nanostructures prepared by wet chemical method. *Ceram. Int.* **2014**, *40*, 523–529. [[CrossRef](#)]
53. Ali, D.; Butt, M.Z.; Muneer, I. Synthesis and characterization of sol-gel derived La and Sm doped ZnO thin films: A solar light photocatalyst for methylene blue. *Thin Solid Film* **2019**, *679*, 86–98. [[CrossRef](#)]
54. Asikuzun, E.; Ozturk, O.; Arda, L.; Tasci, A.T.; Kartal, F.; Terzioglu, C. High-quality C-axis oriented non-vacuum Er doped ZnO thin films. *Ceram. Int.* **2016**, *42*, 8085–8091. [[CrossRef](#)]
55. Young, S.L.; Chen, H.Z.; Kao, M.C.; Kung, C.Y.; Lin, C.C.; Lin, T.T.; Horng, L.; Shih, Y.T.; Ou, C.J.; Lin, C.H. Magnetic properties of La-doped and Cu-doped ZnO nanowires fabricated by hydrothermal method. *Int. J. Mod. Phys.* **2013**, *27*, 1362006. [[CrossRef](#)]
56. Li, W.L. *Effect of La/Cu-Doping and Point Defect on the Magnetic and Optical Properties of ZnO by First-Principle*; Inner Mongol University of Technology: Hohhot, China, 2019.

Disclaimer/Publisher’s Note: The statements, opinions and data contained in all publications are solely those of the individual author(s) and contributor(s) and not of MDPI and/or the editor(s). MDPI and/or the editor(s) disclaim responsibility for any injury to people or property resulting from any ideas, methods, instructions or products referred to in the content.